Journal of Computational Sciences.
homepage: https://centerlin.com

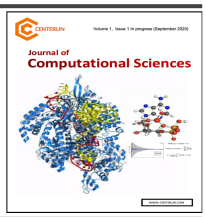

Thermal Conductivity of Zirconium Diboride from Green-Kubo Equilibrium Simulations and the Impact of Point Defects

Jude O. Ighere, Laura de Sousa Oliveira and P. Alex Greaney
School of Mechanical, Industrial & Manufacturing Engineering,
Oregon State University, Corvallis, OR, USA.

ABSTRACT--Transition metal diborides are considered choice materials for thermal applications for its high melting temperatures and shock resistance. ZrB_2 and HfB_2 are found to be advantageous. In here is presented molecular dynamic simulations performed to obtain thermal conductivity using the Green-Kubo method for various point defects (vacancy, interstitials, isotopic). Tersoff potentials are used for atomic interactions and thermal conductivity computed for defective and defect-free ZrB_2. The thermal resistance correlation to number of defects were explored. The simulated structure with point defects is presented. Computed thermal conductivity values showed that interstitial defects are detrimental to thermal transport in ZrB_2 unlike vacancies. The defect formation energies were also investigated. The computed results are comparable to available experimental data and are presented to further the knowledge on ZrB_2 based materials.

1. INTRODUCTION

The correlation between atomic level understanding and macro scale prediction of thermal properties is a critical for technological advancement in leading edges of super-sonic aircraft, complex integrated circuits and advanced nuclear plants [1-5]. As an ultra-high temperature ceramics (UHTC) with melting point of about 3240° C, ZrB_2 is a favorable candidate for advanced thermal engineering. Based on its high thermal conductivity coupled with high melting point, this material offers the possibility of high thermal re-radiation from high temperature regions. Recent data have shown that small changes in the impurity content of ZrB_2-based ceramic resulted in significant thermal conductivity changes [6, 7]. This property combined with its high strength and chemical inertness has been harnessed in different applications including thermal conductivity prediction by intrinsic phonons [18]. Even though ZrB_2 is a conductor, studies have shown that its heat transport mechanism is dominated by phonons [16,18, 23]. It is essential to develop a structure-property multi-correlation for ZrB_2 materials. In this article, we predict thermal conductivity changes in theoretical materials in which defects dominate phonon scattering lifetimes. This has been done by modeling thermal transport using the Boltzmann transport equation in which the mean free paths of phonons are modeled as a function of wave vector and polarization, and how these scattering processes interact with the extreme anisotropy of the $ZrBr_2$ crystal structure. To this end, in this work we use a combination of classical molecular dynamics and Boltzmann transport theory to: (1) characterize the intrinsic thermal transport in ZrB_2, (2) compute structures and energies of point defects in ZrB_2, (3) Compute the thermal conductivity and phonon lifetimes in defected ZrB2 and finally (4) Quantify the phonon scattering cross-section of defects to phonons of different wave.

The significant impact of tungsten particles on the thermal conductivity of titanium diboride reported in recent articles raises concerns for other transition metal diborides such as zirconium diboride [22, 25, 26]. Other researchers have reported varying thermal conductivity values for zirconium diboride ranging from 56 W/(mK) to about 133 W(mK) at room temperatures. However, the source of disparities in the thermal properties of zirconium diboride remain unclear [6, 22, 25-27]. One could propose that imperfections and impurities in structure based on processing technique of ZrB_2 and different sources of component elements play a role. There are enormous amounts of defect types to investigate in a bid to harness thermal properties of ZrB_2, however in this paper point defects are the focus.

2. BONDING AND LATTICE STRUCTURE

ZrB_2 belong to the family of hexagonal isostructural transition metal diborides (TMB_2) with a AlB_2-type 4d crystal structure with space group P6/mmm [8]. The structure is a repeating layer of boron atoms with the zirconium atoms arranged in an alternating hexagonally closed packed layer. The unusual properties of this material have been attributed to its multi-bonding types in the structure. The boron-layered structure is similar to the hexagonal planes of carbon atoms in graphite but unlike carbon, boron atom only has three valence electrons. Like carbon atom in graphite, boron bonds to its nearest neighbor boron atoms to form strong σ-bond within the planes and weak π-bond

between planes. Thus, since there are only three valence electrons available in a boron atom, some of the σ-bonds are not filled. Therefore, researchers have attributed the characteristic stiffness of ZrB_2 unit cell to the strong boron-boron covalent bonds and the thermal conductivities to the metallic bonds [10]. This disparity in stiffness of the different bond types along with the large mass difference between B and Zr creates distinct bands of high and low frequency lattice vibrations [9].

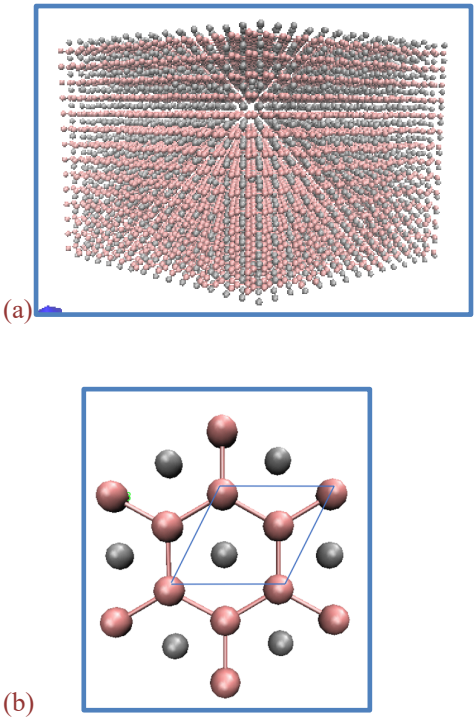

Fig. 2.1: Zirconium diboride lattice structure, showing (a) alternating layers of Zr and B and (b) front hexagonal [0001] view showing the space group

To develop an atomistic understanding of defect impacts (types and concentrations) on the thermal properties, an optimized structure of perfect ZrB_2 was first obtained as in Fig. 2.1. Fig. 2.1 (a) shows the slice of alternating layers of individual species stacked in the hexagonal structure (see Fig. 2.1b). The non-clustered atoms demonstrating position integrity of each atom type in the lattice. The within layer Zr-Zr metallic bond is visually depicted without bond lines while the B-B within layer bond stiffness with thick lines, represents the strong sigma bond.

3. CHARACTERIZING DEFECT STRUCTURE

Three groups of defects have been considered in this study: vacancies, interstitials and isotopic defects. Fig. 3.1 shows the nature of the resulting point defects, clustering out-of-place Zr-interstitial, and in-plane B-interstitial. Zr interstitial (see fig. 3.1a and b) pulls adjacent Zr atoms creating a pseudo-cluster of defect. Zr vacancy (see fig. 3.1c and d) in the crystal lattice creates an in-plane atomic size void. While B interstitial deforms the B-B hexagonal structure without intra-plane interaction (fig. 3.1e and f). Like Zr, boron vacancy maintains structural integrity while creating atomic size void (fig. 3.1g and h). ZrB_2 stiffness attributed to the B-B within layer bond strength is visible in its lattice point integrity [27]. Boron interstitials forms monolayer bond with nearest atoms without protruding clusters unlike the zirconium interstitial clusters which form interlayer bonding. Boron-11 and zirconium-97 were used for the isotopic defects in the lattice structure. All defects were introduced first generating a 6x6x9 unit cell dimension in LAMMPS with periodic boundaries in all directions. The structure was relaxed and energy of the system computed before defect introduction. Point defects were introduced and the structure was relaxed again using energy minimization before computing new energy of the system.

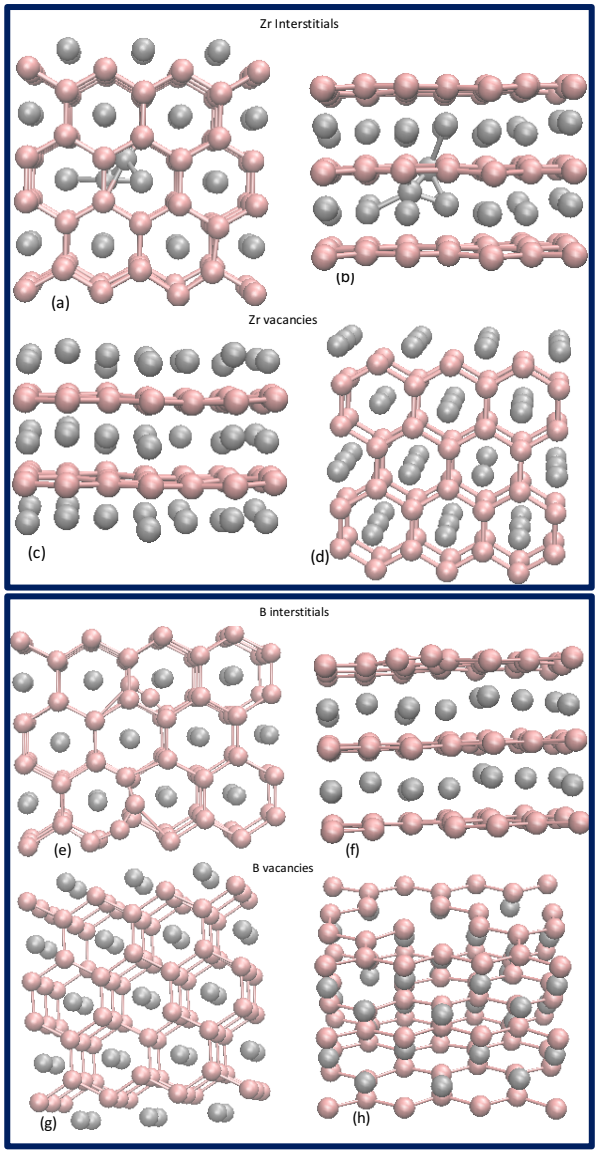

Fig. 3.1 Depiction of the defects computed in this work: (a-b) Zr interstitial and (c-d) Zr vacancy while (e-f) B interstitial and (g-h) B vacancy.

Each defect type was created and then annealed by heating to 900K and then cooled slowly to 300K at 5psi before quenching and relaxing the structure. The energy of each defect was computed and the hessian matrix of the atoms in the vicinity of the defect computed. The computed change in cohesive energy of the system was used to calculated the energy of defect formation. The defect formation energies were used to justify the likelihood of formation of specific defects type. The energy attributed to the defect was calculated by

$$E_d = E_D - \frac{N_D}{N_o} E_o \qquad (1)$$

where E_D *and* E_o represents the final energy of the defective and defect-free ZrB_2 crystal system while N_D *and* N_o represents the number of atoms in the defective and defect-free ZrB_2 crystal system respectively. Fig. 3.2 presents the energy values for the various defects types considered. A study by Martin et al. shows that it cost increased energy to create vacancies for Ti and Zr due to increased valence electrons unlike Nb and Mo. [29]. Other studies only consider the enthalpy of formation of ZrB_2. Increasing positive energy of formation for both interstitial and vacancy with the number of defects (see Fig. 3.2) could be attributed stiffness in ZrB_2 crystal lattice. Fig. 3.1(g-i) depicted that the atomic sites of Zr in the lattice are non-deviating, thereby forcing the interstitial atoms out of the Zr-Zr plane (intra-layer).

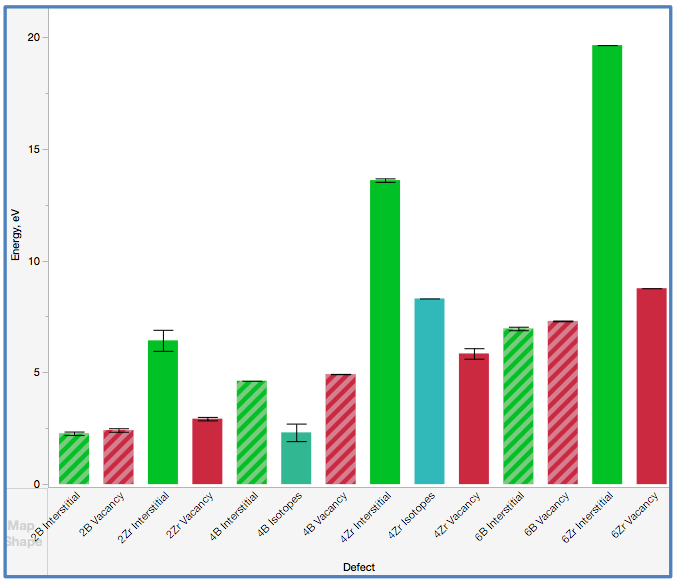

Fig. 3.2 Corresponding energies for interstitials, vacancies and isotopic defects. The interstitials and vacancies are shown in Fig. 3.1.

4. CALCULATION OF THERMAL CONDUCTIVITY

Lattice thermal conductivity is the elastic effect of its vibration (phonons). There are two techniques that have been established and commonly used to compute the thermal conductivity of materials using MD simulations. These are (1) the Green-Kubo Method (an equilibrium method), and (2) the simulation of heat transport under an imposed temperature gradient (non-equilibrium method). These are the Green-Kubo Method (or equilibrium method), direct method using Fourier's law of heat conduction (non-equilibrium). The heat current autocorrelation function shows fluctuation about zero at equilibrium and therefore Green-Kubo method computes thermal conductivity based on the time it takes for the fluctuations to dissipate quantified by computing the integral of the heat current autocorrelation function [11, 12]. Green-Kubo expression for thermal conductivity is given by

$$\kappa = \frac{V}{k_B T^2} \int_0^\infty \mathbf{J}(t).\mathbf{J}(t+\tau)\, d\tau, \qquad (2)$$

where $\boldsymbol{J}(t).\boldsymbol{J}(t+\tau)$ is termed the heat autocorrelation function, and **J** is the heat current vector. Green Kubo (GK) Theorem has been used extensively in studying the thermal conductivity of solid materials but very limited analysis on zirconium diboride and its family of anisotropic ceramics. The GK method connects the integration of the ensemble average of the heat current correlation function to the lattice thermal conductivity tensor, κ_{ij} is given by [13]

$$\kappa_{ij} = \frac{V}{k_B T^2} \int_0^\infty J_i(0).J_j(\tau) d\tau, \qquad (3)$$

where V is the system volume, k_B is Boltzmann constant, and T is the system temperature. The Green Kubo (GK) method has been used extensively in studying the thermal conductivity of solid materials including in defect-free zirconium diboride and its family of anisotropic ceramics [5-8, 16, 22]. The heat current vector can be calculated at time t, from the spatial configuration as: $J(t) = \frac{1}{V}\left[\sum_i e_i v_i + \sum_{i<j}(f_{ij}.v_j)x_{ij}\right]$, where i and j represent atom i and neighbor j, v_j is the velocity of atom i, e_i is the per atom energy of atom i, f_{ij} is the force on atom i due to atom j and x_{ij} is the vector from x_i to x_j. Kaburaki et al. showed that the accuracy of the Green-Kubo method large depends on the interatomic potential used for its implementation [15]. To simulate ZrB_2 using molecular dynamics, the proper super cell and interatomic potential is required. Murray et al. have used Tersoff interatomic potentials for modeling Zr, Hf, and B properties and demonstrated repeatability. These potentials have been reported to be stable across multiple test for different properties of these diborides [24]. In our study, we have adopted this well-defined potential to investigate the thermal properties of perfect ZrB_2 lattice structure and to determine the additional thermal resistance due to point defects.

Following Daw et al. simulation for perfect ZrB_2 was performed with 6 x 6 x 9 supercell for the prediction of thermal conductivity, k [16]. In this study, however, initial gross analysis simulations were performed at 300K using different super cell sizes to predetermine optimal thermal conductivity values along the axial directions computed for perfect ZrB_2. LAMMPS code were used to perform the MD simulation. The optimal 6 x

6 x 9 supercell boxes were created and simulated. The system was simulated in NPT ensemble to sweep average volumetric expansion as a function of time under zero pressure. The system was them fixed at its average system dimensions at 300K and equilibrated in NVT ensemble at specified temperatures. This was followed by NVE ensemble to further equilibrate the system before starting to record the heat current autocorrelation. Low timesteps of 0.5e-3 fs was used to optimize sampling rate within one oscillation and maintain energy conservation at the specific simulation temperature range (300 -2100K) (i.e. minimizing fluctuation). Each system configuration was simulated at least five times for improved data mean and control for variability in initial velocities. Another challenge of Green-Kubo (GK) is the convergence of the heat current (flux) indicating time for system equilibration. Recent studies have highlighted the relevance heat flux integral contribution (see equation 2.1) in predicting the thermal conductivity based on duration of the oscillation [17, 18]. However, researchers have presented different views on how much oscillation time is sufficient and its significance to thermal diffusivity.

After system equilibration, autocorrelation of the heat flux was computed from the time series data from longer simulation time to reduce statistical noise. The averaged data from multiple correlation was considered to converge within 35ps of simulation time. Green-Kubo method uses the trapezoidal rule to integrate the heat current autocorrelation function (HCAF) $< J_i(0).J_j(\tau) >$ as expressed in equation 2. The normalized autocorrelation function (ACF) is shown in fig. 4.2

4.1 Size Convergence

The hexagonal closed packed unit cell of ZrB_2 presents an opportunity to create data file of different box sizes. Defect-free crystalline system of ZrB_2 of different box dimension were investigated for thermal conductivity values as presented in Fig. 4.1. Simulations were performed for different system configurations to understand the size effect on the thermal values. Fig. 4.1a correlates the thermal conductivities of 3 x 3 x 3 and a larger supercell 9 x 9 x 15 across temperature range (200-2100K). The supercell size is less impactful on the κ values. There is a wide variation in the computed thermal conductivity (κ) ranging from 45-194 W/(mK) as presented in Fig.4.1b with box size configuration starting from 3 x 3 x 3 to 15 x 15 x 15 at 300K. It is interesting to note that in the x and y direction, thermal conductivity decreased with increasing box length. Thermal conductivity, κ values were recorded on 6 x 6 x 9 supercell dimensions. Along the z-axis there is no conclusion on impact of box length on κ values. Studies have shown that there are directionally dependent thermal properties [19], however in this case our study is to optimize the average thermal conductivity by first performing size convergence. The average κ (Fig. 4.1a) is close to reported experimental data [20] but the contribution in each axial direction was not reported. Also, critical to using Green-Kubo is the convergence of the heat current autocorrelation function (HCAF).

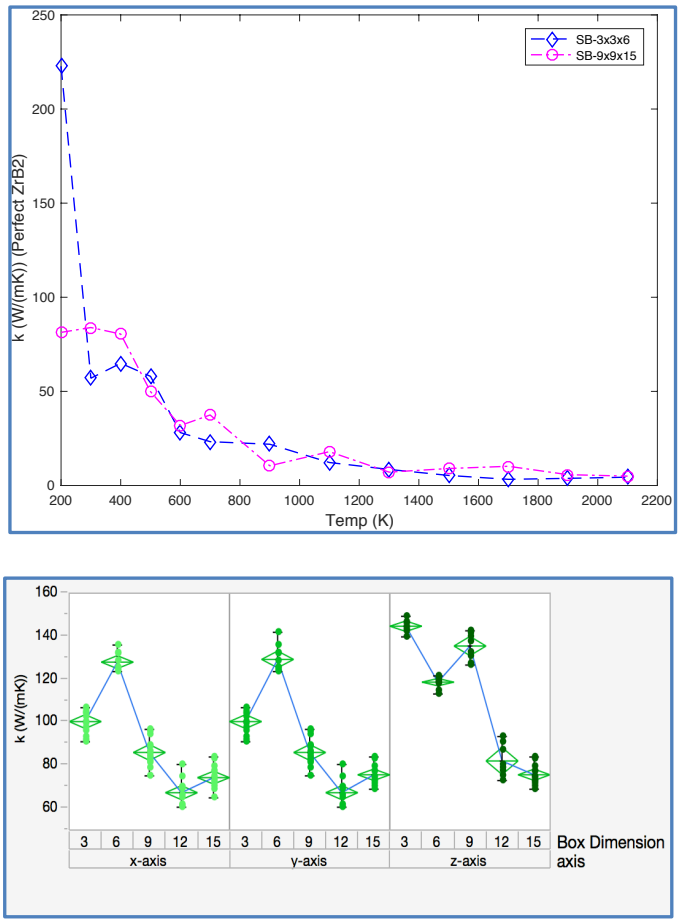

Fig. 4.1. In (a) thermal conductivity, κ for ZrB_2 in different supercell sizes across temp range (b) is the directional k along the basal x and y directions and z-direction at 300K.

4.2 HCCF Convergence

Fig. 3.2 presents the normalized accumulated average of the HCCF. The result below only shows the defect-free crystalline ZrB_2 at T=300K as a control for variability due to defects in subsequent simulations. The simple moving average model for the time series was applied to analyze the computed heat current. The decay and frequency of oscillation is similar on the basal direction along x and y but different from the decay in the z-direction. Although the initial oscillation in the z-direction is regular but converges faster. From Fig. 3.2b, z-direction shows a slower convergence with high oscillations between ~23 - 30ps and re-converges. It demonstrates why the simulation time should be truncated to prevent any accumulation of noise over longer time, similar approach was adopted by L. S. Oliveira in the study of thermal properties of graphite [30]. Along the x- and y-axis, long lasting simulation is required due to slower but more regular decay. The HCCFxx result is comparable to that obtained by Lawson et al [16] but does not present the HCCF along y and z directions. The simulation times was sufficient

(a)

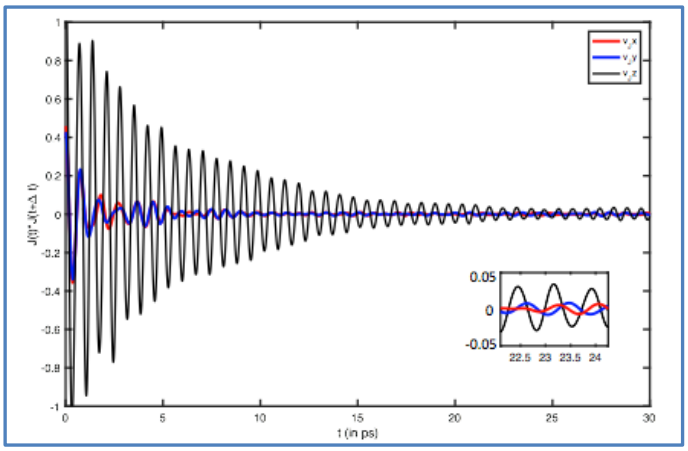

Fig. 4.2. the normalized HCACF computed overlay along xyz-axis for perfect ZrB_2

for heat flux convergence along all axial directions and therefore the result is computed with relatively minimum noise, at which T=300K is about 127W/(mK) on average. Other methods have been reported to use longer and shorter simulation times to compute thermal conductivity. However, true thermal conductivity can only be computed at infinite simulation time, to include all average fluctuations.

4.3 Thermal Conductivity of Defected ZrB_2

Previous articles have reported thermal conductivity trend for ZrB_2 with temperature but no characterization of thermally resistive processes due to point defects [20, 21]. Experiments have also shown differences in measured κ values for single crystal and polycrystalline ZrB_2, attributed mostly to grain boundaries resistance in polycrystalline [23]. Here we computed κ values in the presence of different point defects class in ZrB_2 using a 6 x 6 x 9 supercell sizes at 300K. Thermal conductivities for vacancies and isotopes were higher than interstitial defects both for boron (B) and zirconium (Zr) (see Fig. 4.3). While Zr atoms interstitials measured κ values from 24.6, 13.9 and 5.4 W/(mK) for two, four and six interstitial atoms respectively, B atoms interstitials recorded 4.57, 11.3 and 6.72 W/(mK). For vacancy defects, measured κ values were higher than that for perfect ZrB_2 structure. Computed κ 183 and 198 W/(mK) respectively for two B and two Zr vacancies. Lee et al also recorded increased conductivity due to vacancy defects in graphene but attributed to changes in localized electrons. Also, recent study by Oliveira and Greaney suggests the presence of localized modes for certain defect types [30, 31]. Significant differences in the results can be attributed to changes in the frequency of vibrational modes but there is more work to determine how this influence the heat flux in the different spatial or

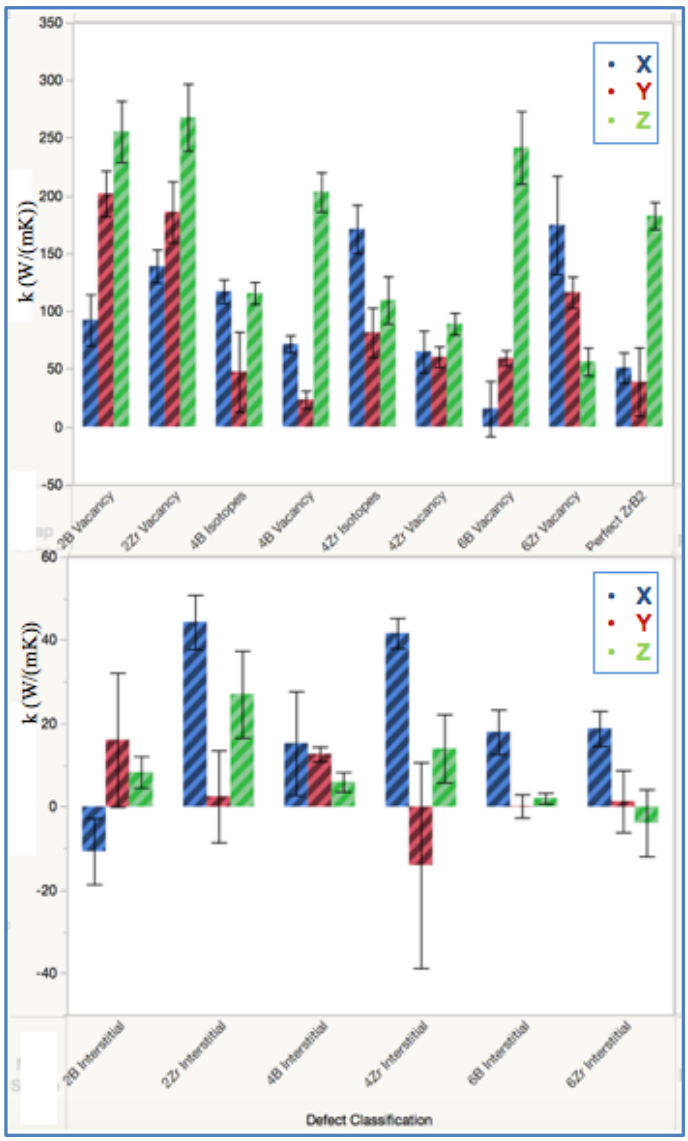

Fig. 4.3. κ values for different ZrB_2 defect systems at room temperature, (top) shows κ for vacancies and isotopes, and (bottom) shows κ interstitials in the x, y, z-directions.

axial direction. The vacancy and isotopic defects increased κ values in the z-direction and proportional change in the basal direction. Similar results were obtained using a different supercell size hence the results may be dependent on the interlayer spacing and defect alignments. It is unclear if the B vacancies allow for a stronger lattice vibration of the σ-bonds [9], however, the absence of B would constitute a stronger Zr-Zr metallic bond and thereby increasing thermal conductivity [10].

Experimental estimate at 300K by Devon Lee [20] measured 88 W/(mK) and the simulation results are in agreement for perfect ZrB_2 structure. This κ value is lower than 108

W/(mK) for sintered ZrB_2 measured by Zhang et al. These κ values are comparable to results at low temperatures [9, 20-23]. The results presented in Fig. 4.3 do not indicate that thermal conductivity largely vary with the number of defects but rather the type of defects and potentially the spacing. There are little notable differences in the κ values computed along the z-direction compare to the basal directions for the various defect types. The injection of these defects is expected to change neighbor orientations, bond types and lengths. These characteristic changes are anisotropic and impact directionally dependent components such as the heat flux. In Fig. 4.4, the anisotropic ratio computed for the basal directions is presented for the various ZrB_2 classifications. Studies have not shown the changes in frequency modes to appropriately characterize thermal conductivity degeneracy or upswing.

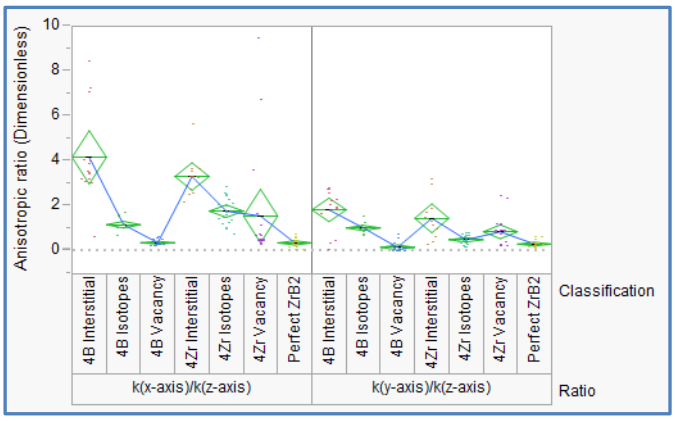

Fig. 4.4. Anisotropic ratio computed for the basal directions (x and y) in relation to z for the defect types.

Thermal conductivity values on Fig 4.3 indicate that the spatial orientation of the defect could be different and therefore pose variation in the overall conductivity of the system. There is a dependence of κ on the type of defects whether interstitial or vacancy. However, there is little difference with regards to the number of interstitials or vacancies. Influence of an extra B-atom or the absence of it on the σ-bond within B plane and weak Π-bond intra-plane is reflected in the change in κ value recorded. In determining the resistance imposed by these defects relative to defect-free ZrB_2, the Mathieson's rule was applied. If defect is considered a source of phonon scattering, according to Mathieson's rule the total resistivity is the sum of resistivity due to the defects and the resistivity due to the lattice vibration in the crystal structure. Therefore, the imposed thermal resistance (r) due to defect is calculated as shown below:

$$r_{defective} = r_{perfect} + r_{defects} \quad (3)$$

But thermal resistance, r = 1/κ, of the system

$$r_{defect} = \frac{1}{\kappa_{Defective}} - \frac{1}{\kappa_{Perfect}} \quad (4)$$

For Mathieson's rule to be applicable, the scattering contribution from each defect would be additive. The additive contribution to the thermal resistance due to defect is given as $r_{defect} = r_{defective} - r_{perfect}$. Fig. 4.5 presents the computed thermal resistance for a system size without defect ($r_{perfect}$) and one with point defects ($r_{defective}$). It therefore suggests that the same system size with double the number of defects would be in the form $r_{defective-2} = r_{perfect} + 2.r_{defects}$. The resistivity of the two interstitial Zr and B defects system are 0.09 and 0.24 mK/W$x10^{-3}$ respectively. However, the respective resistivity of four interstitial defects are 0.08 and 0.11 mK/W$x10^{-3}$. Therefore, doubling the number of point defects does not correspondingly double thermal resistance. It is however, worth noting that there are no data at this time regarding how the orientation and stacking of the defects will change the resistivity contribution in the system.

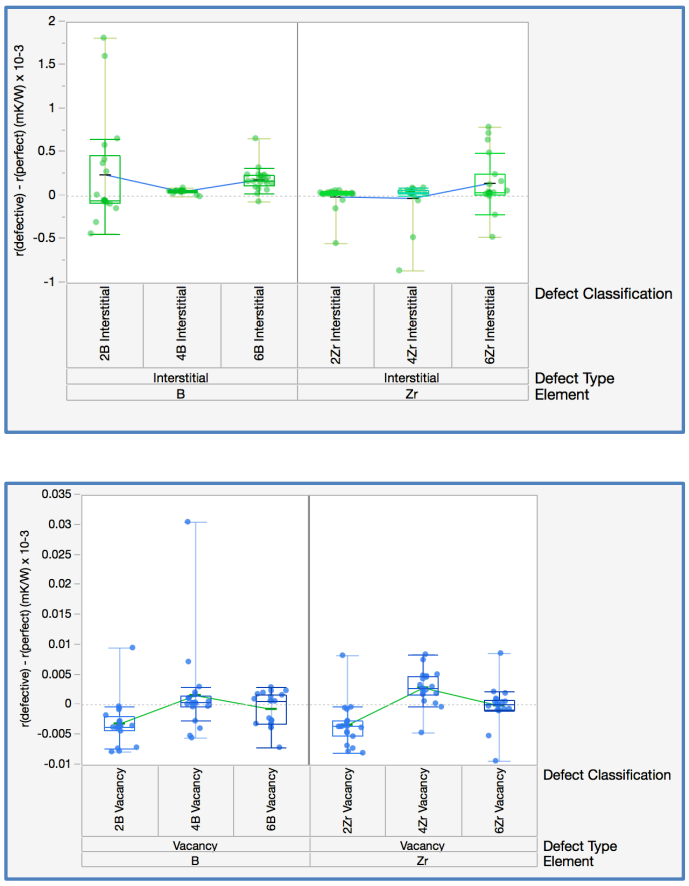

Fig. 4.5. Independent thermal resistance contribution of (top) B and Zr interstitial (bottom) B and Zr vacancies in ZrB_2 system

5. SUMMARY AND CONCLUSIONS

In this study, we have reported the thermal conductivity of both defect-free and imperfect ZrB_2 by Green-Kubo simulations. Perfect crystal lattice of ZrB_2 is different from real crystal

structure due to variation in densification processes and nature of synthetic powder. Vacancy defects, packing and interstitials are common to real ZrB_2 materials. With an optimized 6 x 6 x 9 supercells, the Green-Kubo approach was used, and autocorrelation function converged within 35ps correlations time. Frequency of oscillation and decay in the z-direction is different from basal direction. At 300K vacancy defects gave higher thermal conductivity than defect-free ZrB_2 while interstitial defects lowered the thermal conductivity. The integrity of the lattice sites in the Zr interlayer, force the interstitial atoms to position between adjacent layers. Computed values of thermal conductivity below 750K (Debye temperature) are consistent with literature. Higher temperatures did not show significant difference with defect types, which could be attributed to size of the simulated system. In addition to computing the trend in thermal conductivity due to defects, we have correlated the change in cohesive property in terms of energy of ZrB_2 crystal system with defect formation. There is increased energy required for interstitial and vacancy defect formation with the number of defects.

ACKNOWLEDGEMENTS

This work used Oregon State University computing resources and also resources of the Bioinformatics Computational Research Group in University of California Riverside.

REFERENCES

[1] Bansal, Narottam P., ed. (2004). *Handbook of Ceramic Composites*. Springer. p. 192.

[2] Salute, Joan; et al. (2001). *SHARP-B 2: Flight Test Objectives, Project Implementation and Initial Results*. 2nd Annual Conference on Composites, Materials and Structures, Cocoa Beach, FL, United States.

[3] Agarwal, D. C., and U. Brill, "Material Degradation Problems in High Temperature Environments," *Industrial Heating,* p. 56 (Oct. 1994).

[4] A. Jankowiak, J.F. Justin. Ultra-High Temperature Ceramics for aerospace applications. *ODAS 2014*, Jun 2014, COLOGNE, Germany. <hal-01103216v2>

[5] Sylvia M. Johnson. Ultra-High Temperature Ceramics: Applications, Issues and Prospects. NASA-Ames Research Center. 2nd Ceramic Leadership Summit Baltimore, MD. August 3, 2011

[6] Zimmermann, J. W., Hilmas, G. E., Fahrenholtz, W. G., Dinwiddie, R., Porter, W., and Wang, H. "Thermophysical Properties of ZrB2-Based Ceramics" Journal of the American Ceramic Society 91, no. 5 (2008):1405-1411.

[7] Hilmas, G. E., Fahrenholtz, W. G., Talmy, I. G., and Zaykoski, J. A. "Refractory Diborides of Ziconium and Hafnium" Journal of the American Ceramic Society 01, no. 5 (2007):1347-1364.

[8] Wangsheng Chu[a, b], Ziyu Wu[b, d,], Wenhan Liu[a], N.L. Saini[c], A. Bianconi[c], Tiandou Hu[b], Yaning Xie. Lattice dynamics study of AlB2-type 4d transition-metal diborides by extended X-ray-absorption fine structure. Radiation Physics and Chemistry. Volume 127, (October 2016) .

[9] Hyoung Joon Choi*, David Roundy*†, Hong Sun*, Marvin L. Cohen*† & Steven G. Louie (2002). The origin of the anomalous superconducting properties of MgB2. Nature. Vol 418 (2002)

[10] J. W. Zimmermann, G. E. Hilmas, and W. G. Fahrenholtz, "Thermophysical Properties of ZrB2 and ZrB2-SiC Ceramics," *Journal of the American Ceramic Society,* 91[5] 1405-11 (2008).

[11] Melville S. Green. Markoff random processes and the statistical mechanics of time dependent phenomena. ii. irreversible processes in fluids. The Journal of Chemical Physics, 22(3), 1954.

[12] Rajiv Asthana; Ashok Kumar; Narendra B. Dahotre (9 January 2006). Materials Processing and Manufacturing Science. Butterworth–Heinemann. pp. 158–. ISBN 978-0-08-046488-6. Retrieved 7 May 2013.

[13] D. A. McQuarrie, Statistical Mechanics. University Science Books, Sausalito (2000) 520-521.

[14] Vijaya & Rangarajan and Gopala Rangarajan. Materials Science. Tata McGraw- Hill Education, February 2004. ISBN 0070534691.

[15] H. Kaburaki, J. Li, S. Yip, and H. Kimizuka, J. Applied Physics 102,043514 (2007)

[16] J. W. Lawson, M. S. Dawson and C. W. Bauschlicher, Jr. Lattice thermal conductivity of ultra high temperature ceramics ZrB_2 and HfB_2 from atomistic simulation. Journal of Applied Physics, 110, 083507 (2011).

[17] Laura de Sousa Oliveira, P. Alex Greaney. Thermal resistance from irradiation defects in graphite. Computational Materials Science 103 (2015) 68–76

[18] D. P. Sellan, E. S. Landry, J. E. Turney, A. J. H. McGaughey, and C. H. Amon. Size effects in molecular dynamics thermal conductivity predictions. Phys. Rev. B 81, 214305 – Published 21 June 2010

[19] William A. Paxton,1 Tevfik E. Özdemir,1 İlyas Şavklıyıldız, Terence Whalen, Hülya Biçer, Enver Koray Akdoğan, Zhong Zhong, and Thomas Tsakalakos1. Anisotropic Thermal Expansion of Zirconium Diboride: An Energy-Dispersive X-Ray Diffraction Study. Journal of Ceramics Volume 2016 (2016), Article ID 8346563

[20] McClane, Devon Lee, "Thermal properties of zirconium diboride - transition metal boride solid solutions" (2014). Theses. Paper 7265.

[21] H. Kinoshita, S. Otani, S. Kamiyama, H. Amano, I. Akasaki, J. Suda and H. Matsunami. Zirconium Diboride (0001) as an Electrically Conductive Lattice-Matched Substrate for Gallium Nitride. Japanese Journal of Applied Physics, Volume 40, Part 2, Number 12A.

[22] J. W. Zimmermann, G. E. Hilmas, W. G. Fahrenholtz, R. B. Dinwiddie, W. D. Porter, and H. "Thermophysical

Properties of ZrB2-Based Ceramics" Wang. Journal of the American Society. Vol. 91, 1405 (2008)

[23] Zhang, D. A. Pejaković, J. Marschall, and M. Gasch, "Thermal and Electrical Transport Properties of Spark Plasma-Sintered HfB2 and ZrB2 Ceramics," Journal of the American Ceramic Society, 94[8] 2562-70 (2011).

[24] Murray S. D., John W. L., and Charles W. B. Interatomic potentials for Zirconium Diboride and Hafnium Diboride. Computational Material Science 50 (2011) 2828-2835.

[25] Thompson, M. J., Fahrenholtz, W. G., and Hilmas, G. E. "Elevated Temperature Thermal Properties of ZrB2 with Carbon Additions" Journal of the American Ceramic Society 1085, (2012)

[26] Clougherty, E. V, Wilkes, K. E, and Tye, R. P. "Research and Development of Refractory Oxidation-Resistant Diborides" (1969).

[27] S. Guo, T. Nishimura, and Y. Kagawa, "Preparation of zirconium diboride ceramics by reactive spark plasma sintering of zirconium hydride–boron powders," Scripta Materialia, 65[11] 1018-21 (2011).

[27] Middleburgh, Simon C.; Parfitt, David C.; Blair, Paul R.; Grimes, Robin W. (2011). "Atomic Scale Modeling of Point Defects in Zirconium Diboride". Journal of the American Ceramic Society. 94 (7): 2225–2229

[28] Zhi Wang and Zhanjun Wu. Fabrication, Microstructure, and Properties of Zirconium Diboride Matrix Ceramic. Dalian University of Technology, China. Source Title: MAX Phases and Ultra-High Temperature Ceramics for Extreme Environments. (2013) 59. DOI: 10.4018/978-1-4666-4066-5.ch012

[29] Martin Dahlqvist, Ulf Jansson and Johanna Rosén, Influence of boron vacancies on phase stability, bonding and structure of MB2 (M = Ti, Zr, Hf, V, Nb, Ta, Cr, Mo, W) with AlB2 type structure, 2015, Journal of Physics: Condensed Matter, (27), 43, 435702.

[30] L. S. Oliveira, P. A. Greaney, Thermal resistance from irradiation defects in graphite. Computational Materials Science 103 (2015) 68–76.

[31] Geunsik Lee, Kwang S. Kim, and Kyeongjae Cho, Theoretical Study of the Electron Transport in Graphene with Vacancy and Residual Oxygen Defects after High-Temperature Reduction. J. Phys. Chem. C, 2011, 115 (19), pp 9719–9725